12th International Symposium on Turbulence and Shear Flow Phenomena (TSFP12)
Osaka, Japan (Online), July 19-22, 2022

INFLUENCE OF WALL SHEAR STRESS ON THE SECONDARY FLOW IN SQUARE DUCTS

Alexander Doehring
Technical University of Munich
TUM School of Engineering and Design
Chair of Aerodynamics and Fluid Mechanics
Boltzmannstr. 15, 85748 Garching, Germany
alex.doehring@tum.de

Thomas Kaller and Steffen J. Schmidt and Nikolaus A. Adams
Technical University of Munich
TUM School of Engineering and Design
Chair of Aerodynamics and Fluid Mechanics
Boltzmannstr. 15, 85748 Garching, Germany
thomas.kaller@tum.de
steffen.schmidt@tum.de
nikolaus.adams@tum.de

ABSTRACT

We investigated turbulent duct flows with a square cross section using well-resolved large-eddy simulations (LES). A physically consistent subgrid-scale turbulence model is incorporated, that is based on the Adaptive Local Deconvolution Method (ALDM) for implicit LES. The wall shear stress is artificially modified at one of the four walls to mimic different surface properties. A direct numerical simulation (DNS) of a symmetrical duct flow is used as reference to asses the influence of a modified wall shear stress. The modification results in an asymmetrical distribution of the secondary flow source terms, affecting the momentum distribution. Further, the anisotropy of the Reynolds stress tensor, which induces the secondary flow vortices is considerably affected by the wall shear stress change.

Introduction

Turbulent flow within a straight duct with a rectangular cross section is of great importance for many engineering applications. This includes for instance ventilation systems, cooling channels in rocket engines, nuclear reactors and heat exchangers. A thorough understanding of the turbulent flow is necessary in order to predict the cooling efficiency, the pressure drop and the system lifetime. These properties are highly affected by the specific manufacturing technology that is employed, since it determines the wall surface properties. Especially additive manufacturing processes provide the possibility for new design options of a product, but introduce rougher surfaces. The roughness parameters are affected by the production parameters as for instance the build direction. In order to investigate the effect of an asymmetric wall roughness variation on the square duct flow field, we performed well-resolved LES simulations with an artificially modified wall shear stress at one of the four walls.

Turbulent flows through rectangular ducts are affected by turbulence induced secondary flow, also known as Prandtl's flow of the second kind. The flow is characterized by a vortex system consisting of a counter rotating vortex pair in each corner. According to Salinas Vázquez & Métais (2002) the secondary flow of the second kind is relatively weak with a strength of approximately $1-3\%$ of the bulk flow, but it increases the mixing by transporting high momentum fluid from the duct core to the corners. The secondary flow is induced due to the anisotropy of the Reynolds stress tensor (Demuren & Rodi (1984)). Thus, turbulence models using the isotropic eddy viscosity ansatz fail. Demuren & Rodi (1984) analysed the generation of Prandtl's flow of second kind using the streamwise vorticity equation. They determined that gradients of the anisotropic Reynolds stress tensor act as source term for the vorticity production. The influence of the duct geometry on corner vortex system has been investigated by Vinuesa *et al.* (2014), performing DNS of different aspect ratio duct flows. They observed an array of secondary vortices along the long sidewalls. Vidal *et al.* (2017) investigated the influence of round corners in duct flows on the secondary flow. Unexpectedly, rounding the corner did not reduce the secondary flow, but the magnitude of the cross-flow was similar compared to sharp corners ducts.

Modelling difficulties were shown by Vane & Lele (2015) performing wall-modelled LES with an equilibrium wall-model for different duct flows. Their results were improved by introducing the Buleev length scale and adjusting the coupling point, but the wall shear stress distribution was not matching the DNS results. For this reason, they obtained a shifted vortex system, as it is strongly affected by the wall shear stress distribution. Based on our well-resolved LES we are investigating the role of the wall shear stress for the secondary flow.

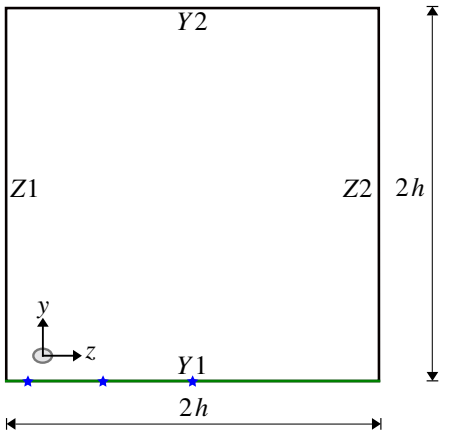

Figure 1: Cross section of the computational domain. The walls are labelled and the modified lower y-wall (Y1) is indicated green. The stars are locations which are used for further evaluation with $z/h = -0.9$, $z/h = -0.5$, $z/h = 0$ from left to rigth.

Numerical Model

LES simulations are performed solving the three-dimensional, fully compressible Navier-Stokes Equations. The ideal gas law is used to close the system and the viscosity is modelled by the Sutherland law. For time advancement an explicit second-order low-storage four-stage Runge-Kutta method with enhanced stability region is applied (Schmidt *et al.* (2006)). The governing equations are spatially discretized on a block structured, curvilinear grid using the finite-volume method. Viscous fluxes are discretized by a linear second-order centered scheme. Convective fluxes are determined using a compact four cell stencil by Egerer *et al.* (2016). The switch between the two schemes is made by sensor functionals. The convective flux calculation is based on the Adaptive Local Deconvolution Method (ALDM), which is a nonlinear finite volume method, that provides a physically consistent subgrid-scale turbulence model for implicit LES, see Hickel *et al.* (2006, 2014).

Setup

We are investigating a generic duct configuration, focusing on the influence of an asymmetric wall shear stress modulation on secondary flow. For this purpose, case C from the DNS study by Pirozzoli *et al.* (2018) with a bulk Reynolds number of $Re_b = 17800$ and a friction Reynolds number $Re_\tau = 519$ is used. The wall shear stress of the lower wall in y direction is artificially changed by multiplying the obtained shear stress within the simulation by a constant factor. This adjustment is used to mimic a variation of surface properties. Periodic boundary conditions are used in streamwise direction. The walls are isothermal and a no slip boundary condition is applied. The bulk pressure is set to $p_b = 1.01325\,\mathrm{bar}$. The duct geometry is $10h \times 2h \times 2h$ in streamwise, wall-normal and spanwise direction with the duct half height h, respectively. We use a hyperbolic mesh distribution in wall-normal directions and a uniform grid in the streamwise direction. All simulations have been performed on the same grid with $N_x = 117$, $N_y = 88$, $N_z = 88$ cells. Table 1 provides the obtained resolution with respect to wall units $\Delta y^+ = h_y^+ = \Delta y \rho_w u_\tau / \mu_w$,

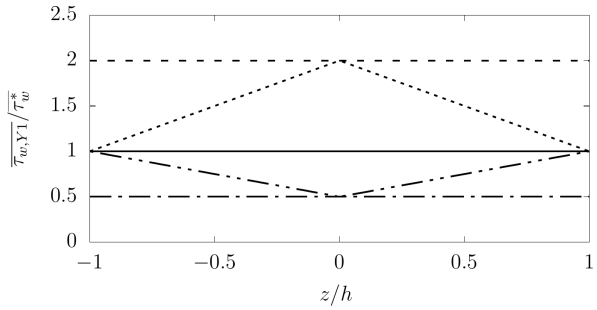

Figure 2: Intended mean wall shear distribution for different cases. The perimeter-averaged wall shear stress $\overline{\tau_w^*}$ of LES_P is used for normalization. The lines correspond to LES_P (———), LES_T+ (− − − −), LES_T- (− · − · −), LES_L+ (·····), LES_L- (− ·· − ··).

Table 1: Summary of resolution parameters.

$h^+_{y_{\min,\mathrm{Y1}}} \times h^+_{y_{\min,\mathrm{Y2}}}$	1.554215×1.130634
$h^+_{y_{\max,\mathrm{Y1}}} \times h^+_{y_{\max,\mathrm{Y2}}}$	$31.114517 \times 22.634663$
$h^+_{z_{\min,\mathrm{Z1}}} \times h^+_{z_{\min,\mathrm{Z2}}}$	1.122118×1.119152
$h^+_{z_{\max,\mathrm{Z1}}} \times h^+_{z_{\max,\mathrm{Z2}}}$	$22.464188 \times 22.464188$

with the friction velocity $u_\tau^2 = (\tau_w/\rho_w)$ and the wall shear stress $\tau_w = (\mu \partial u/\partial y)|_w$. Here, the wall shear stress is averaged over each wall and the resolution is based on the whole cell size, but the flow variables are evaluated at the cell center. Therefore, the effective minimum wall distance is $\Delta y_{\min}/2$. The values in the table represent the highest values obtained from all five simulations. The domain is shown in figure 1. The walls are labelled and the modified wall Y1 is highlighted in green. A forcing source term in the momentum and energy equations ensures a constant bulk velocity and the respective bulk Reynolds number. The additional body force is based on Brun *et al.* (2008). First, a LES of case C is performed without modifications labelled LES_P (Pirozzoli), that serves as a reference. Four more LES are performed with a modified wall shear stress $\tau_{w,mod}(Y1) = C(y) \times \tau_{w,orig}$. Two LES simulations contain a wall shear stress which is augmented (LES_T+) and decreased (LES_T-) by a factor of two, compared to LES_P. Thus, $C(y) = 2$ and $C(y) = 0.5$. In the remaining two LES the wall shear stress is linearly increasing (LES_L+) and decreasing (LES_L-). The intention is to obtain a linear distribution with a minimum and maximum value at the center, which corresponds to simulation LES_T+ and LES_T-. The targeted wall shear stresses for the performed LES are shown in figure 2. Note, that the actual profiles will decrease towards $z/h = \pm 1$ due to the influence of the sidewalls.

Results

At first we evaluate the mean flow field by averaging in streamwise direction and in time after reaching a quasi-stationary state. Mean values are indicated with an overbar and fluctuations with a prime. The mean velocity profiles are presented in figure 3. The profiles are extracted at wall Y1

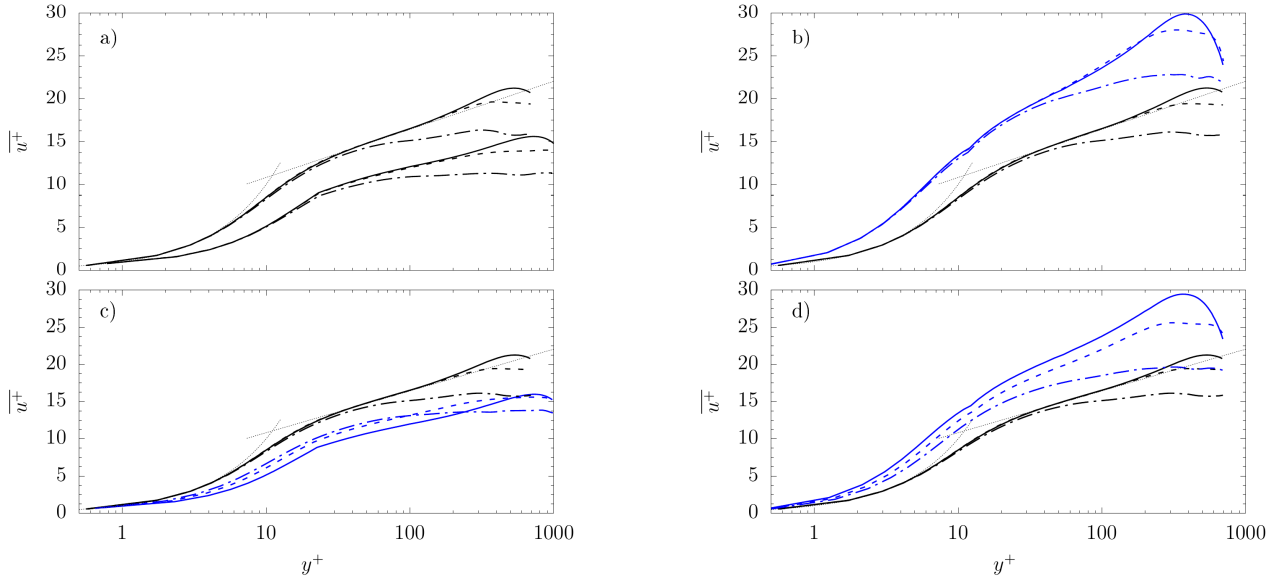

Figure 3: Scaled mean velocity $\overline{u^+}$ over wall units y^+ at wall Y1. The black lines indicate LES_P and the blue lines the modified wall with a) LES_T+, b) LES_T-, c) LES_L+, d) LES_L-. Different line styles correspond to different wall positions including $z/h = 0$ (———), $z/h = -0.5$ (− − − −) and $z/h = -0.90$ (−·−·−). The law of the wall (·····) is included with $\overline{u}^+ = 1/0.41 \cdot \ln y^+ + 5.2$.

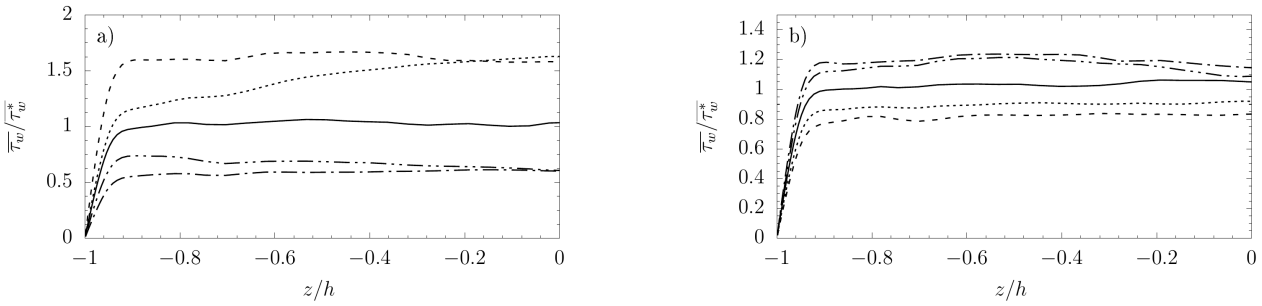

Figure 4: Mean wall shear stress at wall Y1 in a) and wall Y2 in b). The profiles are normalized with the perimeter-averaged wall shear stress $\overline{\tau_w^*}$ of each individual LES. The lines correspond to LES_P (———), LES_T+ (− − − −), LES_T- (−·−·−), LES_L+ (·····), LES_L- (−··−··).

at three different positions, $z/h = 0$, $z/h = -0.5$ and $z/h = -0.9$. The law of the wall velocity profile consists of the viscous sublayer $\overline{u}^+ = y^+$ and logarithmic region $\overline{u}^+ = 1/\kappa \cdot \ln y^+ + B$, with $\kappa = 0.41$ and $B = 5.2$. Based on LES_P it is observed, that at the center of wall Y1 the normalized velocity profile follows the law of the wall. Approaching the side wall results in a flattening of the profile. At $z/h = -0.5$ the profile is identical with the profile at the channel center until $y^+ \approx 200$, with a flattening in the outer layer due to secondary flow. This can also be observed for the constant value cases LES_T+ and LES_T- in figure 3a,b). For $z/h = -0.9$ the flattening affects the whole logarithmic layer. Both cases with an increased wall shear stress (LES_T+, LES_L+) feature a downward shift of the velocity profile as it can be observed in rough channel flows, cf. Thakkar *et al.* (2018). In general, an approach of the wall shear stress towards the value of LES_P results in an approach of the velocity profile towards the law of the wall superimposed with the local secondary flow effect.

The obtained wall shear stress at wall Y1 and Y2 is presented in figure 4. As already mentioned, the stress is decreasing towards the sidewalls at $z/h = \pm 1$. Furthermore, the obtained absolute stress values do not match the intended ones, cf. figure 2. This is a consequence of the perimeter-averaged wall shear stress ($\overline{\tau_w^*}$) of each individual LES which is used here for normalization. For instance, $\overline{\tau_w^*}$ of LES_T+ is higher due to the modification compared to $\overline{\tau_w^*}$ of LES_P resulting in a maximum value of ≈ 1.6 and not 2. Although the secondary flow is not strong, it is capable to alter the wall shear stress distribution. This can be seen in terms of the dent at $z/h \approx -0.7$ leading to a peak value close to the corner and at $z/h \approx -0.5$. This is also observed in DNS studies as for example in Pirozzoli *et al.* (2018) and Zhang *et al.* (2015).

Due to the one-sided modification of the wall shear stress, the mean cross-sectional velocity distribution $\overline{u}_{cf} = \sqrt{\overline{v}^2 + \overline{w}^2}$ becomes asymmetrical compared to the symmetrical LES_P, compare figures 5a)-d) with 5e). When the wall shear stress is reduced the vortices at the modified wall Y1 are getting smaller, weaker and are pushed towards the corners, whereas the vortices at the opposite wall Y2 are expanding into the lower duct half, see 5b). The vortices at the sidewalls Z1 and Z2 are getting stronger and bigger. The opposite effect occurs for an increase of the wall shear stress at Y1. A linear $C(y)$ distribution intensifies the previous observations made at Y1 and Y2. Interestingly, the intensification is not observed for the vortices at the sidewalls, since they are weaker compared to the constant value modification. This coincides with the

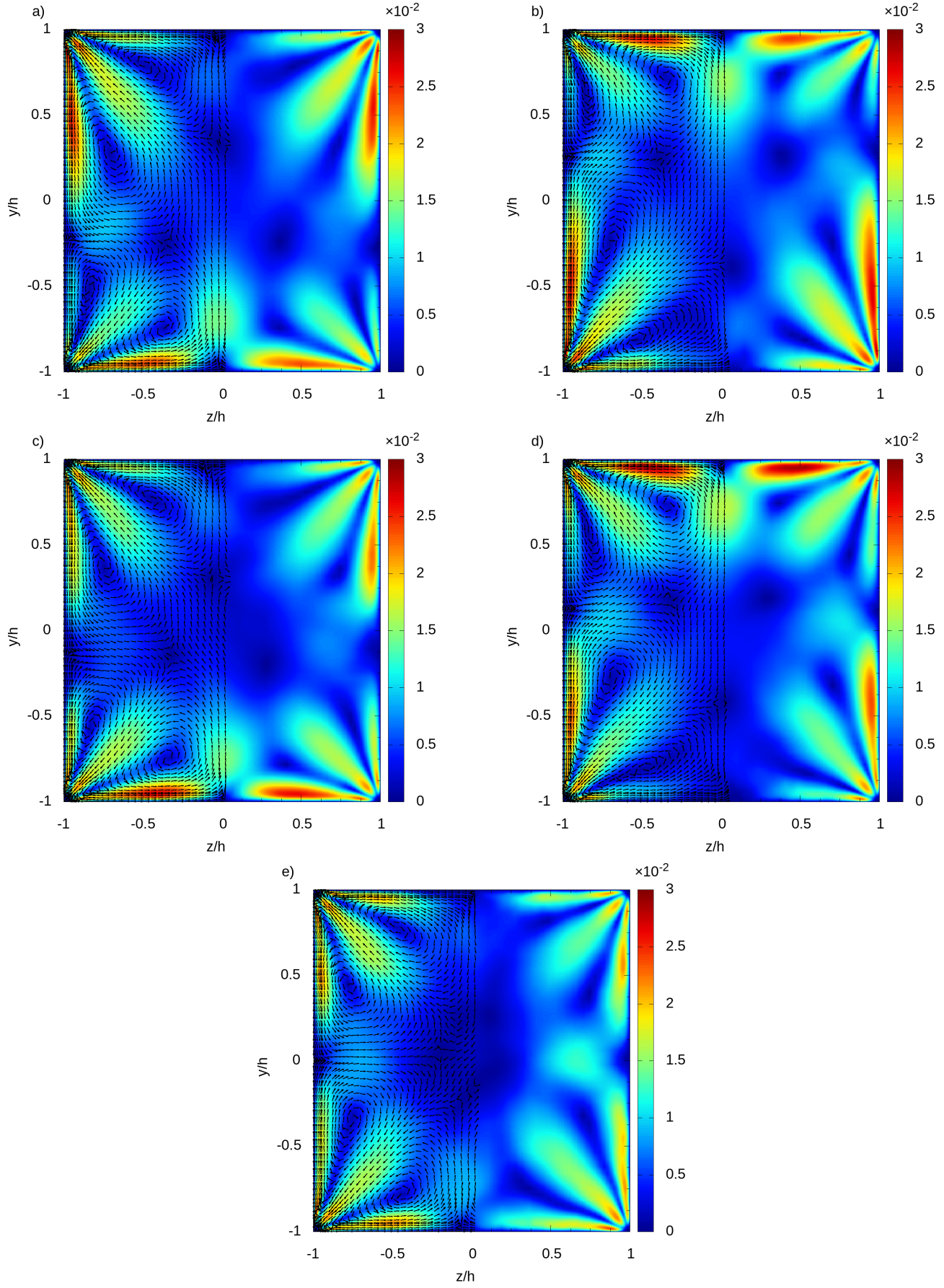

Figure 5: Mean cross-sectional velocity distribution with $\overline{u}_{cf} = \sqrt{\overline{v}^2 + \overline{w}^2}$. a) LES_T+, b) LES_T-, c) LES_L+, d) LES_L- and e) LES_P. The counter-rotating corner vortex system is visualized by velocity vectors.

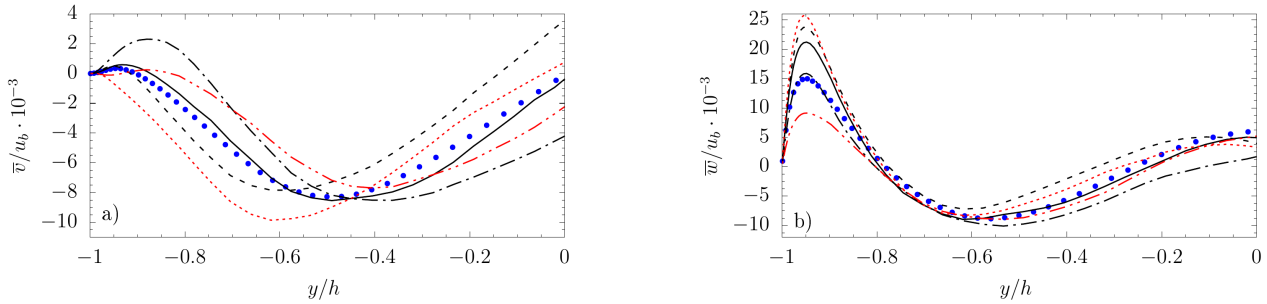

Figure 6: Mean secondary flow $\overline{v}$ and $\overline{w}$ normalized with the bulk velocity u_b at Y1 for $z/h = -0.5$. The lines correspond to LES_P (———), LES_T+ (– – – –), LES_T- (–·–·–), LES_L+ (·····), LES_L- (–··–··), and DNS data from Pirozzoli *et al.* (2018) (●).

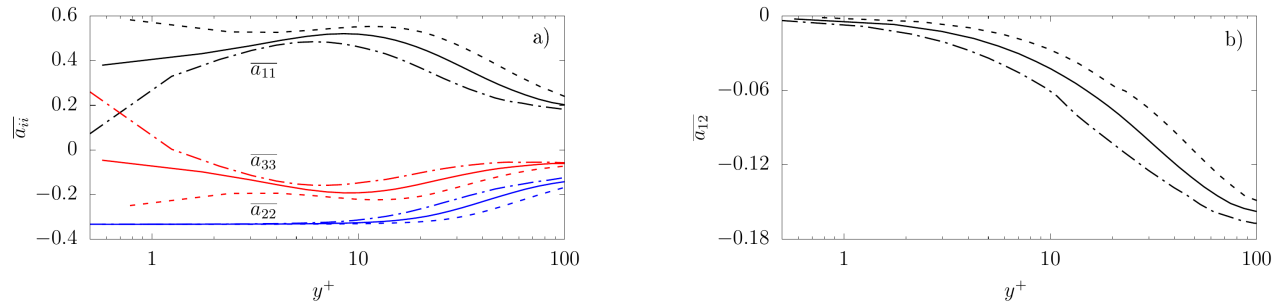

Figure 7: Distribution of diagonal components a) and off-diagonal components b) of the Reynolds stress anisotropy tensor at $z/h = -0.5$. The lines correspond to LES_P (———), LES_T+ (– – – –), LES_T- (–·–·–).

wall shear stress values of the linear modified LES simulations close to the sidewalls, that are approaching LES_P.

The effects of the wall shear stress modification on the mean secondary flow velocities $\overline{v}$ and $\overline{w}$ are shown in figure 6 at $z/h = -0.5$. DNS data from Pirozzoli *et al.* (2018) are included to assess the numerical accuracy of LES_P. The maximum of the wall normal velocity $\overline{v}$ close to Y1 refers of the two smaller corner vortices pushing fluid upwards and the following minimum refers to the two larger corner vortices pushing fluid downwards. The tangential velocity $\overline{w}$ transports fluid from the duct corner to the midplane. LES_P is in good agreement with the DNS data with a slight overestimation of the vortex intensity close to the wall. The modification of $\overline{\tau_w}$ mainly changes the intensity of $\overline{w}$ whereas the peak position remains fixed and for $\overline{v}$ both the intensity and peak position are altered. These observations can be similarly made for asymmetrical wall heating, which modifies the wall shear stress as well as the turbulence intensities due to viscosity modulation. Kaller *et al.* (2019) showed that a heated wall for water is weakening the intensity of the counter rotating vortices. An $\overline{\tau_w}$ increase moves the vortices closer into the corner and a $\overline{\tau_w}$ decrease away from the corner, see 6a). This is similarly shown in the contour plots of figure 5. The observed shrinkage of the vortex at Y1 from LES_P over LES_T- to LES_L- in figure 5 is reflected in the reduction of the maximum value for $\overline{w}$.

A study by Patel *et al.* (2016) demonstrated the influence of density and viscosity gradients on turbulence using the anisotropy tensor, which is defined as

$$\overline{a_{ij}} = \frac{\overline{u_i' u_j'}}{2k} - \frac{\delta_{ij}}{3}, \tag{1}$$

with the turbulent kinetic energy $k = \overline{u_l' u_l'}$ and δ_{ij} the Kronecker delta. Figure 7 presents the components of the anisotropy tensor influenced by the wall shear stress. Patel *et al.* (2016) demonstrated that any change in viscosity or density has only a marginal effect on the wall normal component $\overline{a_{22}}$. This also holds for changes in the wall shear stress up to the buffer layer at approximately $y^+ = 10$. An increase of $\overline{\tau_w}$ results in a higher anisotropy value for the streamwise component $\overline{a_{11}}$ and a decrease for the tangential component $\overline{a_{33}}$ compared to the unmodified LES. The opposite is the case for a decrease of the wall shear stress. The ratio between the turbulent kinetic energy and turbulent shear stress indicates the momentum transfer in figure 7b). Using a higher wall shear stress as in case LES_T+ causes a higher momentum transfer. Further, we apply the anisotropy-invariant map (AIM) in figure 8 (Emory & Iaccarino (2014)). Here, the Lumley triangle defines the borders of all possible states and the 2nd invariant ($I_2 = a_{ij}a_{ji}/2$) and the 3rd invariant ($I_3 = a_{ij}a_{jn}a_{ni}/3$) of the Reynolds stress tensor are used as axis. A higher anisotropy for an increased $\overline{\tau_w}$ is also observed in AIM, since LES_T+ starts closer and gets closer to the one-component (1-C) limit. The opposite is the case for a decrease of the wall shear stress. In addition, a kink is present for LES_+ starting at the 2-component edge close to the 1-C limit, moving along the edge towards the 2-component axis-symmetric limit(2-C) and turning again towards 1-C, see zoom in figure 8a). This phenomenon is also observed close to the sidewall at $z/h = -0.9$ in figure 8b) but not for LES_T- and LES_P.

Conclusion

We have performed well-resolved LES simulations of a turbulent straight duct flow with a rectangular cross section. A physically consistent subgrid-scale turbulence model based on the Adaptive Local Deconvolution Method (ALDM) for implicit LES was incorporated. The wall shear stress $\overline{\tau_w}$ was arti-

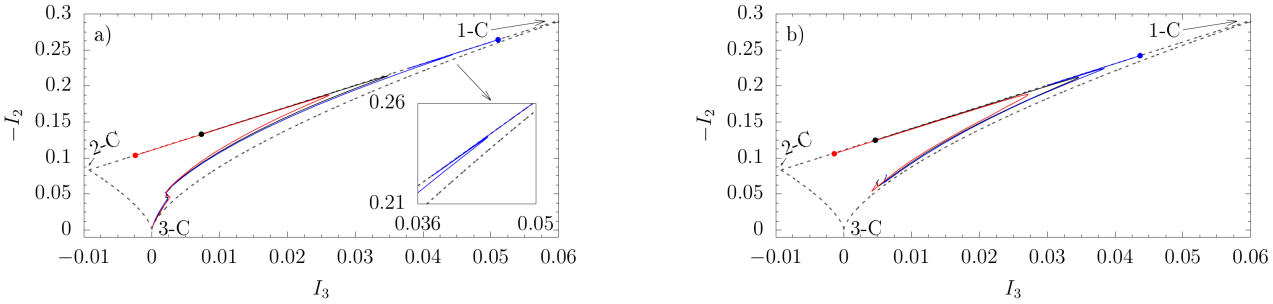

Figure 8: Reynolds stress anisotropy invariant map evaluated at $z/h = 0$ a) and $z/h = 0.9$ b). The lines correspond to LES_P (———), LES_T+ (– – – –), LES_T- (–·–·–). The lines start at the modified wall Y1 indicated with dots and the limiting states are defined by the Lumley triangle.

ficially modified at one of the four walls in order to investigate the effect of an asymmetric wall roughness variation on the square duct flow field. A LES simulation based on the DNS study by Pirozzoli *et al.* (2018) was used to assess the influence of the modified wall shear stress. Four modifications have been considered, consisting of two with a constant decrease and increase of $\overline{\tau_w}$ and two with a linear decrease and increase of $\overline{\tau_w}$. The analysis of the law of the wall showed a flattening of the velocity profile while approaching the sidewalls. Based on the cross-sectional velocity distribution we observed that the vortices at the modified wall are getting smaller, weaker and are pushed towards the corners whereas the vortices at the opposite wall are expanding into the lower duct half. Using a linear profile intensifies the observations made at the modified wall but only a moderate strengthening or weakening was present at the sidewalls. Furthermore, the modification of $\overline{\tau_w}$ has mainly led to a change in intensity of the secondary flow velocity $\overline{w}$ whereas the peak position remain fixed. For $\overline{v}$ both the intensity and peak position have been altered. The anisotropy of the Reynolds stress tensor was investigated by means the anisotropy invariant map and the tensor components. A higher wall shear stress causes a higher anisotropy which consequently led to an increase in the strength of the secondary flow since the are induced by the anisotropy of the Reynolds stress tensor.

Acknowledgments

The authors gratefully acknowledge the financial support provided by the German Research Foundation (Deutsche Forschungsgemeinschaft-DFG) within the framework of the Sonderforschungsbereich Transregio 40, SFB-TRR40 (Technological foundations for the design of thermally and mechanically highly loaded components of future space transportation systems). Computational resources have been provided by the Leibniz Supercomputing Centre Munich (LRZ).

REFERENCES

Brun, C., Boiarciuc, M. P., Haberkorn, M. & Comte, P. 2008 Large eddy simulation of compressible channel flow. *Theoretical and Computational Fluid Dynamics* **22**, 189 – 212.

Demuren, A. O. & Rodi, W. 1984 Calculation of turbulence-driven secondary motion in non-circular ducts. *Journal of Fluid Mechanics* **140**, 189–222.

Egerer, C. P., Schmidt, S. J., Hickel, S. & Adams, N. A. 2016 Efficient implicit LES method for the simulation of turbulent cavitating flows. *Journal of Computational Physics* **316**, 453–469.

Emory, M. & Iaccarino, G. 2014 Visualizing turbulence anisotropy in the spatial domain with componentality contours. *Center for Turbulence Research Annual Research Briefs* pp. 123–138.

Hickel, S., Adams, N. A. & Domaradzki, J. A. 2006 An adaptive local deconvolution method for implicit LES. *Journal of Computational Physics* **213**, 413–436.

Hickel, S., Egerer, C. P. & Larsson, J. 2014 Subgrid-scale modeling for implicit large eddy simulation of compressible flows and shock-turbulence interaction. *Physics of Fluids* **26**.

Kaller, T., Pasquariello, V., Hickel, S. & Adams, N. A. 2019 Turbulent flow through a high aspect ratio cooling duct with asymmetric wall heating. *Journal of Fluid Mechanics* **860**, 258–299.

Patel, A., Boersma, B. J. & Pecnik, R. 2016 The influence of near-wall density and viscosity gradients on turbulence in channel flows. *Journal of Fluid Mechanics* **809**, 793–820.

Pirozzoli, S., Modesti, D., Orlandi, P. & Grasso, F. 2018 Turbulence and secondary motions in square duct flow. *Journal of Fluid Mechanics* **840**, 631–655.

Salinas Vázquez, M. & Métais, O. 2002 Large-eddy simulation of the turbulent flow through a heated square duct. *Journal of Fluid Mechanics* **453**, 201–238.

Schmidt, S. J., Sezal, I. H. & Schnerr, G. H 2006 Compressible simulation of high-speed hydrodynamics with phase change. In *European Conference on Computational Fluid Dynamics*. TU Delft, The Netherlands.

Thakkar, M., Busse, A. & Sandham, N. D. 2018 Direct numerical simulation of turbulent channel flow over a surrogate for nikuradse-type roughness. *Journal of Fluid Mechanics* **837**.

Vane, Z. P. & Lele, S. K. 2015 Prediction of turbulent secondary flows in ducts using equilibrium wall-modeled les. In *53rd AIAA Aerospace Sciences Meeting*, p. 1274.

Vidal, A., Vinuesa, R., Schlatter, P. & Nagib, H. M. 2017 Influence of corner geometry on the secondary flow in turbulent square ducts. *International Journal of Heat and Fluid Flow* **67**, 69–78.

Vinuesa, Ricardo, Noorani, Azad, Lozano-Durán, Adrián, Khoury, George K El, Schlatter, Philipp, Fischer, Paul F & Nagib, Hassan M 2014 Aspect ratio effects in turbulent duct flows studied through direct numerical simulation. *Journal of Turbulence* **15** (10), 677–706.

Zhang, H., Trias, F. X., Gorobets, A., Tan, Y. & Oliva, A. 2015 Direct numerical simulation of a fully developed turbulent square duct flow up to reτ= 1200. *International Journal of Heat and Fluid Flow* **54**, 258–267.